2018 European Control Conference (ECC)
June 12-15, 2018. Limassol, Cyprus

A Real-time Nonlinear Air Path Observer for Off-Highway Diesel Engines

Karsten Harder*, Michael Buchholz**, Tim Späder* and Knut Graichen**

Abstract— **Air path observation is important for the diagnosis and control of modern diesel engines. Recent air path observers assume the measurement of the mass air flow which is a justified assumption in the automotive domain. However, the mass air flow is usually not measured for series-produced off-highway engines as the pipework is customized. Due to the intense complexity of the air path, a tailored spherical simplex unscented Kalman filter is used to achieve real-time feasibility. In order to consider the dependency of the air path model uncertainty from the engine operating point, a nonlinear residual based adaptation scheme for the measurement noise covariance matrix is proposed. The high accuracy and the computational performance of the observer is demonstrated by GT-POWER simulation runs, testbench measurements, and a running time analysis.**

I. INTRODUCTION

Due to continuous development and stricter emission laws, modern diesel engines are highly complex systems. Model based methods can be used to handle the complexity efficiently. However, the chemical reactions during the combustion mainly correlate with air path quantities that cannot be measured in series-produced engines, e.g. the exhaust gas recirculation (EGR) ratio that is essential for the control of nitrogen oxides (NO_x) [1], [2], [3].

The air path state reconstruction for off-highway diesel engines with high accuracy is challenging for several reasons. First, these diesel engines only have some basic sensors for controlling the air path, e.g. pressure, temperature, and turbocharger speed. Nevertheless, exhaust pressure sensors are not suitable for series-produced engines due to the exposure to particulate matter as well as to high temperatures. Second, mass air flow (MAF) sensors are not common for off-highway diesel engines as their pipework is customized. Next, the air path of an off-highway diesel engine is more complex in comparison with an automotive engine, e.g. there are several turbochargers and additional flaps. Finally, the observer must be real-time feasible on an engine control unit (ECU) within the short sampling time in engine control, typically in the range of 5 to 10 ms.

There are different approaches for air path observation that are tailored to the air path, sensor setup, and quantities that should be estimated. For instance, a model reference identification algorithm for the estimation of the EGR ratio is proposed and validated experimentally in [4]. The estimation is based on a simple first order (quasi-)linear parameter varying (LPV) model of the air path. However, the dependency of the system parameters on the state dynamics is neglected. Thus, the high accuracy of the corresponding nonlinear model cannot be represented sufficiently accurate. Similar LPV models are used for the observers suggested in [5] and [6]. Moreover, the LPV approach is based on MAF measurement.

In [7], the combination of an online optimization and an unscented Kalman filter (UKF) is suggested for simultaneous air path observation and parameter estimation using a nonlinear model. Experimental results demonstrate a good observation accuracy, where real-time feasibility on a rapid prototyping system was achieved within a sampling time of 100 ms. In addition, the observer is based on MAF measurement, which significantly facilitates the air path observation. Another UKF approach is employed in [8] for EGR ratio estimation of a marine diesel engine. Indeed, the required sensor and air path configuration is suitable for an off-highway diesel engine, but the approach has only been validated by simulations against the same model as used for observation.

In this contribution, a nonlinear air path observer is presented that is tailored to off-highway diesel engines. As the computational effort for the observation mainly depends on the model complexity, a zero-dimensional (nonlinear) air path model is used [1], [2], [3]. Further improvements in terms of real-time feasibility are achieved using a spherical simplex UKF that needs a minimum number of model evaluations. A high estimation accuracy is obtained using the full sensor information related to the air path, e.g. intake pressure and temperature, exhaust temperature, air-fuel ratio, and NO_x. Though the measurement of NO_x is standard in engine control, it is non-standard to use it for the reconstruction of the air path states as it assumes the existence of a nitrous oxide model, but useful as EGR highly correlates with NO_x. In addition, the air path model uncertainty depends on the engine operating point, e.g. due to pressure pulsations that influence the measurements. Thus, the estimation quality is enhanced by a novel nonlinear residual-based adaptation scheme for the measurement noise covariance matrix. The observer is validated against a high fidelity GT-POWER model of the engine to demonstrate the quality of its estimation for the relevant states that cannot be easily measured on a test bench. Experimental validation data is also used to demonstrate high performance of the observer estimating the exhaust pressure. The observer is additionally implemented on a rapid prototyping system to estimate the computation time for a prospective ECU implementation.

*K. Harder and T. Späder are with MTU Friedrichshafen GmbH, Germany {karsten.harder, tim.speader}@mtu-online.com

** M. Buchholz and K. Graichen are with the Institute of Measurement, Control and Microtechnology, Ulm University, Germany {michael.buchholz, knut.graichen}@uni-ulm.de

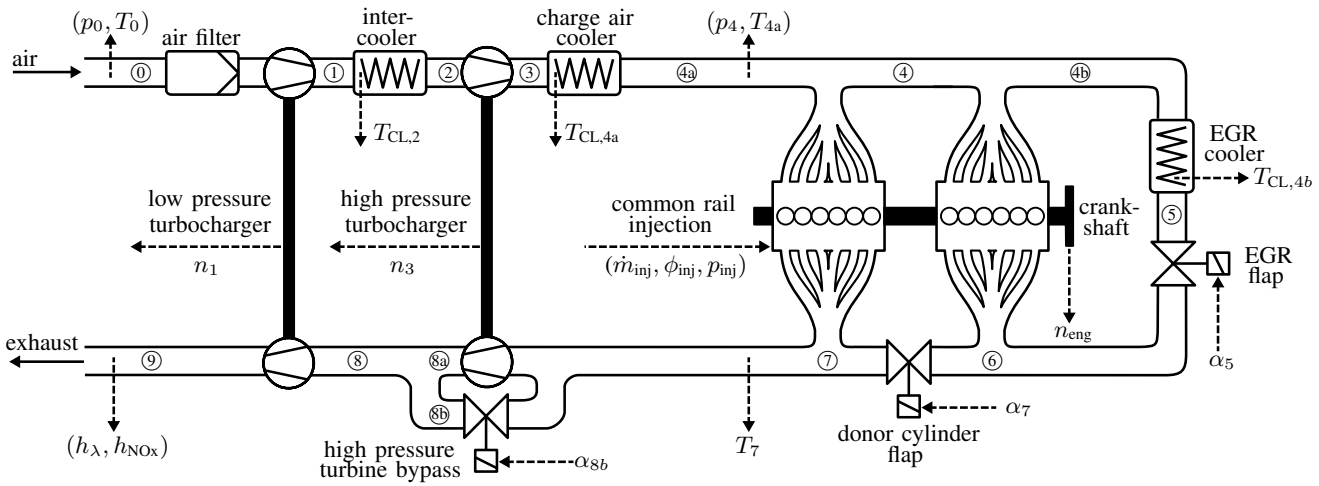

Fig. 1: Schematic of the considered off-highway diesel engine with two turbochargers and exhaust gas recirculation.

II. Modeling

The air path considered in this contribution corresponds to an off-highway diesel engine that is equipped with two turbochargers and exhaust gas recirculation. In the following, a tailored air path model is derived to facilitate the design of a real-time observer.

Fig. 1 shows the schematic of the engine. Filtered ambient air enters the low pressure compressor driven by the corresponding turbine. As the air heats up by compression, an intercooler is employed to increase the air mass flow. Further compression of the charge air is achieved by the high pressure turbocharger and the charge air cooler. Before flowing into the cylinders, the air is mixed with recirculated exhaust gas to reduce NO_x emissions. The donor cylinder flap and the EGR flap are used to control the EGR mass flow rate. The remaining exhaust gas drives the turbines, where the high pressure turbine bypass flap is employed to control the airflow rate. Generally, the engine outlet is connected with an aftertreatment system that is omitted in Fig. 1.

The numbers ⓪-⑨ in Fig. 1 denote the segments between the modules, e.g. flaps. This way, e.g., the corresponding pressures p_i, temperatures T_i, and mass flow rates $\dot{m}_{i\to j}$ are labeled by numbers $i, j \in \{0, \dots, 9\}$. Additional letters are used to distinguish branches. For example, $\dot{m}_{7\to 8b}$ denotes the high pressure turbocharger mass flow.

In order to keep the computation time for the air path model short, a zero-dimensional model approach is applied that is based on the methods described in [1], [2], [3]. Moreover, it is assumed that the dynamics for the temperature and turbocharger speeds T_i and (n_1, n_3) is much slower than the pressure dynamics p_i. The pressure losses of the air filter and the coolers are additionally omitted for simplicity. Thus, the resulting air path model comprises five isothermal volumes $V_i, i \in \{2, 4, 6, 7, 8\}$ with the state vector

$$\boldsymbol{x}^{\mathrm{T}} = \begin{bmatrix} p_2 & p_4 & p_6 & p_7 & p_8 \end{bmatrix} \tag{1}$$

and corresponding pressure dynamics for the air path

$$\dot{\boldsymbol{x}} = \begin{bmatrix} \frac{RT_2}{V_2}(\dot{m}_{0\to 1} - \dot{m}_{2\to 3}) \\ \frac{R}{V_4}(T_{4a}\dot{m}_{3\to 4a} + T_{4b}\dot{m}_{5\to 4b} - T_4(\dot{m}_{4\to 6} + \dot{m}_{4\to 7})) \\ \frac{RT_6}{V_6}(\dot{m}_{4\to 6} - \dot{m}_{6\to 5} - \dot{m}_{6\to 7}) \\ \frac{RT_7}{V_7}(\dot{m}_{4\to 7} - \dot{m}_{7\to 8a} - \dot{m}_{7\to 8b}) \\ \frac{R}{V_8}(T_{8a}\dot{m}_{7\to 8a} + T_{8b}\dot{m}_{7\to 8b} - T_8\dot{m}_{8\to 9}) \end{bmatrix} \tag{2}$$

that directly follows from the ideal gas law with the universal gas constant R.

The mass flow rates and temperatures in (2) are calculated using static models for the corresponding modules. Based on the (measured) ambient conditions (p_0, T_0) and state $\boldsymbol{x}$, the mass flow rates and temperatures related to the path ⓪-④a depend on the compressors and the corresponding coolers. According to [2], [3], a typical (static) compressor model is

$$T_j = T_i\Big(1 + \eta_{\mathrm{CP},j}^{-1}\Big(\frac{p_j}{p_i}, n_j\sqrt{\frac{T_i^*}{T_i}}\Big)\Big(\frac{p_j}{p_i}^{\frac{\kappa-1}{\kappa}} - 1\Big)\Big) \tag{3a}$$

$$\dot{m}_{i\to j} = \frac{p_i}{p_i^*}\sqrt{\frac{T_i^*}{T_i}}\dot{m}_{\mathrm{CP},j}\Big(\frac{p_j}{p_i}, n_j\sqrt{\frac{T_i^*}{T_i}}\Big) \tag{3b}$$

with $(i, j) \in \{(0, 1), (2, 3)\}$, where $\eta_{\mathrm{CP},j}(\,)$ and $\dot{m}_{\mathrm{CP},j}(\,)$ are 2-D look-up tables for the compressor efficiency and reduced mass flow rate in terms of the pressure ratio p_j/p_i and the normalized turbocharger speed $n_j\sqrt{T_i^*/T_i}$. The normalizations take into account that the look-up tables were originally measured at the inlet temperature T_i^* and pressure p_i^*. The heat capacity ratio of air (or exhaust) and the turbocharger speed are denoted as κ and n_j, respectively. To keep the model complexity low, a constant cooler efficiency $\eta_{\mathrm{CL},j}$ is assumed, i.e.

$$T_j = T_i + \eta_{\mathrm{CL},j}(T_{\mathrm{CL},j} - T_i) \tag{4}$$

with $(i, j) \in \{(1, 2), (3, 4a)\}$ and the coolant temperature $T_{\mathrm{CL},j}$.

The burnt gases in the exhaust manifold with the (measured) temperature T_7 pass the high pressure turbine bypass flap and

turbines. A (static) model for the latter is [2], [3]

$$T_j = T_i\Big(1 + \eta_{\mathrm{TB},j}\Big(\frac{p_i}{p_j}, n_k\sqrt{\frac{T_i^*}{T_i}}\Big)\Big(1 - \frac{p_i}{p_j}^{\frac{1-\kappa}{\kappa}}\Big)\Big) \quad (5)$$

$$\dot{m}_{i\to j} = \frac{p_i}{p_i^*}\sqrt{\frac{T_i^*}{T_i}}\dot{m}_{\mathrm{TB},j}\Big(\frac{p_i}{p_j}, n_k\sqrt{\frac{T_i^*}{T_i}}\Big) \quad (6)$$

with $(i,j,k) \in \{(7,8\mathrm{a},3),(8,9,1)\}$, where $\eta_{\mathrm{TB},j}(\,)$ and $\dot{m}_{\mathrm{TB},j}(\,)$ are 2-D look-up tables for the turbine efficiency and reduced mass flow rate. As stated in [3], a typical model for the bypass flap is

$$\dot{m}_{i\to j} = c_{\mathrm{d},j}(\alpha_j)A_j\frac{p_i}{\sqrt{RT_i}}\psi\Big(\frac{p_i}{p_j}\Big) \quad (7)$$

with $(i,j) = \{(7,8\mathrm{b})\}$, where $c_{\mathrm{d},j}$ is the flaps discharge coefficient depending on the valve position α_j. The valve area and flow function are denoted as A_j and $\psi(\,)$ (see [3] for details). The temperature in front of the low pressure turbine

$$T_8 = \frac{T_{8a}\dot{m}_{7\to 8a} + T_{8b}\dot{m}_{7\to 8b}}{\dot{m}_{7\to 8a} + \dot{m}_{7\to 8b}} \quad (8)$$

is obtained as mixed temperature. Assuming that $T_6 = T_7$, the mass flow rates and temperatures of the EGR path ⑥-④ are calculated analogously using (7) with $(i,j) \in \{(6,7),(6,5)\}$ and (4) with $(i,j) = (5,4\mathrm{b})$. Thus, the intake manifold temperature is

$$T_4 = \frac{T_{4a}\dot{m}_{3\to 4a} + T_{4b}\dot{m}_{6\to 4b}}{\dot{m}_{3\to 4a} + \dot{m}_{6\to 4b}}\,. \quad (9)$$

Finally, a simple model for the engine mass flow rate is

$$\begin{aligned}\dot{m}_{4\to 7} &= \dot{m}_{4\to 6}\\ &= \frac{n_{\mathrm{eng}}V_{\mathrm{D}}p_4}{4RT_4}\lambda_{\mathrm{V}}\Big(\frac{p_6}{p_4}, n_{\mathrm{eng}}, T_4\Big) + \dot{m}_{\mathrm{inj}}\,. \end{aligned} \quad (10)$$

The first part of (10) approximates the engine as volumetric pump (see [1], [3] for details), where n_{eng} and V_{D} denote the crankshaft speed and the displaced volume. Deviations of this simple model are taken into account by the volumetric efficiency function $\lambda_{\mathrm{V}}(\,)$. The second part considers the mass increase by the injection mass flow rate $\dot{m}_{\mathrm{inj}}$.

The model (2) is reformulated as nonlinear function

$$\dot{\boldsymbol{x}} = \boldsymbol{f}(\boldsymbol{x}, \boldsymbol{v}) \quad (11)$$

with the independent variables

$$\begin{aligned}\boldsymbol{v}^{\mathrm{T}} \coloneqq [&\alpha_5 \quad \alpha_7 \quad \alpha_{8\mathrm{b}} \quad p_0 \quad T_0 \quad T_{4\mathrm{a}} \quad T_7 \quad T_{\mathrm{CL},2}\\ &T_{\mathrm{CL},4\mathrm{a}} \quad T_{\mathrm{CL},4\mathrm{b}} \quad n_1 \quad n_3 \quad n_{\mathrm{eng}} \quad \dot{m}_{\mathrm{inj}} \quad p_{\mathrm{inj}} \quad \phi_{\mathrm{inj}}]^{\mathrm{T}}\,. \end{aligned} \quad (12)$$

The elements ϕ_{inj} and p_{inj} in (12) are the begin of injection and injection pressure that have a minor influence on the air path but rather on the emissions and engine torque.

The available sensor measurements are illustrated in Fig. 1 by arrows pointing away from the engine. Nevertheless, only the fast ones are considered in the measurement vector

$$\boldsymbol{y} = \begin{bmatrix} p_4 \\ c_{\mathrm{NOx}} \\ \lambda \end{bmatrix} = \underbrace{\begin{bmatrix} x_2 \\ h_{\mathrm{NOx}}(\boldsymbol{x},\boldsymbol{v}) \\ h_\lambda(\boldsymbol{x},\boldsymbol{v}) \end{bmatrix}}_{=:\boldsymbol{h}(\boldsymbol{x},\boldsymbol{v})}, \quad (13)$$

where c_{NOx} and λ denote the measured NO_x emissions and the air fuel ratio. The measurement function $\boldsymbol{h}(\,)$ contains the corresponding models. A suitable nonlinear emission model $h_{\mathrm{NOx}}(\,)$ that was obtained from a validated GT-POWER model of the engine by parameter identification based on data obtained from design of experiment [9]. The output function for the air fuel ratio

$$h_\lambda(\boldsymbol{x},\boldsymbol{v}) = \frac{\dot{m}_{3\to 4a}}{L_{\mathrm{st}}\dot{m}_{\mathrm{inj}}} \quad (14)$$

directly follows from its definition, where $L_{\mathrm{st}} = 14.5$ denotes the stoichiometric air requirement of diesel.

Eventually, a nonlinear, discrete time, state space representation of the air path is

$$\boldsymbol{x}_{k+1} = \boldsymbol{x}_k + \Delta t\boldsymbol{f}(\boldsymbol{x}_k, \boldsymbol{v}_k) \quad (15a)$$

$$\boldsymbol{y}_k = \boldsymbol{h}(\boldsymbol{x}_k, \boldsymbol{v}_k)\,, \quad (15b)$$

where an Euler discretization with the sampling time Δt is used.

III. Observer design

A. Spherical simplex unscented Kalman filter

The estimation of the air path states $\boldsymbol{x}$, i.e. the volume pressures, is based on the nonlinear state space model (15). In order to facilitate a future ECU implementation, the observer has to be numerically efficient and robust.

In the literature there are several approaches for the state estimation of nonlinear systems. A detailed overview and comparison of established approaches is given in [10]. The most popular one, the extended Kalman Filter (EKF), is based on an online linearisation of the nonlinear system model. The unscented Kalman filter (UKF) [11], however, employs characteristic sigma-points to approximate the means and covariances by transformation using (15) which renders, the UKF more robust against nonlinearities. A significant improvement of the numerical efficiency and stability is obtained using the square-root UKF (SR-UKF) [12].

Typical SR-UKFs are based on $2N+1$ sigma-points, where N denotes the number of states. Most of the computational load results from the frequent evaluation of (15). Thus, the spherical simplex unscented transformation [13] that needs only $N+2$ sigma-points is used in this contribution. The results in [13] show that an equal tracking performance can be achieved this way.

B. Noise adaptation

The measurement noise as well as the modeling errors depend on the operating point of the engine. A possible solution is the adaptation of the measurement and process noise covariance $\boldsymbol{R}_k$ and $\boldsymbol{Q}_k$, respectively. In particular, covariance-matching methods are suitable for real-time applications [14], [15]. Nevertheless, the simultaneous adaptation of both covariances is not recommended for these methods [15] as the estimates for $\boldsymbol{Q}_k$ and $\boldsymbol{R}_k$ depend on each other.

Thus, a reliable (fixed) estimation of $\boldsymbol{Q}_k$ for the air path was calculated based on simulation runs using a validated GT-POWER model of the engine. The conventional adaptive

estimation of $\boldsymbol{R}_k$ based on innovation sequences [16] does not guarantee to have a positive definite solution [14]. Moreover, its update law for $\boldsymbol{R}_k$ is not suitable for the calculation of the noise covariance square-root with the computationally efficient QR decomposition as it involves the subtraction of two positive definite matrices. Instead, numerous Cholesky rank-one downdates would be needed in this case to take account for the subtraction. The residual-based method suggested in [14] does not have these disadvantages. Nevertheless, its derivation is only valid for linear systems. Based on an EKF linearization, the approach can be easily adopted to nonlinear systems. Substituting the EKF by an SS-UKF formulation yields the adaptation law

$$\hat{\boldsymbol{R}}_k = \sum_{i=0}^{M-1} \frac{1}{M} \left(\boldsymbol{y}_{k-i} - \hat{\boldsymbol{y}}_{k-i|k-i}\right)\left(\boldsymbol{y}_{k-i} - \hat{\boldsymbol{y}}_{k-i|k-i}\right)^{\mathrm{T}} + \sum_{j=0}^{N+1} w_j^{(\mathrm{c})} \left(\hat{\boldsymbol{y}}_{k|k} - \boldsymbol{\mathcal{Y}}_{k|k}^{j}\right)\left(\hat{\boldsymbol{y}}_{k|k} - \boldsymbol{\mathcal{Y}}_{k|k}^{j}\right)^{\mathrm{T}} \tag{16}$$

with the measurements $\boldsymbol{y}_k$, the estimated measurements $\hat{\boldsymbol{y}}_{k|k}$ (not predicted), the sigma-points $\boldsymbol{\mathcal{Y}}_{k|k}^{j}$, and the corresponding covariance weight $w_j^{(\mathrm{c})}$. The first sum of the adaptation law (16) approximates the measurement filtering residuals covariance over the moving window of the width M. The second sum is the UKF observation covariance.

Based on the adaptation law (16), we suggest the following computational efficient implementation summarized in Alg. 1. Note that the Cholesky update in Step 3) of Alg. 1 is needed to facilitate a scaled (spherical simplex) unscented transformation [17]. If $w_0^{(\mathrm{c})} > 0$, the matrix to be decomposed can instead be extended by the entry $\sqrt{w_0^{(\mathrm{c})}}\left(\hat{\boldsymbol{y}}_{k|k} - \boldsymbol{\mathcal{Y}}_{k|k}^{0}\right)^{\mathrm{T}}$.

Alg. 1 Adaptation of the square-root of $\boldsymbol{R}_k$

1) Compute spherical simplex sigma-points $\mathcal{X}_{k|k}^{i}$, $i = 0, \ldots, N+1$ for the estimated states $\hat{\boldsymbol{x}}_{k|k}$ as described in [13].
2) Calculate transformed sigma-points $\boldsymbol{\mathcal{Y}}_{k|k}^{i} = \boldsymbol{h}\left(\mathcal{X}_{k|k}^{i}, \boldsymbol{v}_k\right)$, $i = 0, \ldots, N+1$ and observation $\hat{\boldsymbol{y}}_{k|k} = \sum_{i=0}^{M-1} w_i^{(\mathrm{c})} \boldsymbol{\mathcal{Y}}_{k|k}^{i}$.
3) Estimate measurement noise covariance square-root

$$\hat{\boldsymbol{S}}_{\boldsymbol{R},k} = \mathbf{qr}\left\{\begin{bmatrix} \frac{1}{\sqrt{M}}\left(\boldsymbol{y}_k - \hat{\boldsymbol{y}}_{k|k}\right)^{\mathrm{T}} \\ \vdots \\ \frac{1}{\sqrt{M}}\left(\boldsymbol{y}_{k-M-1} - \hat{\boldsymbol{y}}_{k-M-1|k-M-1}\right)^{\mathrm{T}} \\ \sqrt{w_1^{(\mathrm{c})}}(\hat{\boldsymbol{y}}_{k|k} - \boldsymbol{\mathcal{Y}}_{k|k}^{1})^{\mathrm{T}} \\ \vdots \\ \sqrt{w_{N+1}^{(\mathrm{c})}}(\hat{\boldsymbol{y}}_{k|k} - \boldsymbol{\mathcal{Y}}_{k|k}^{N+1})^{\mathrm{T}} \end{bmatrix}\right\}$$

$$\hat{\boldsymbol{S}}_{\boldsymbol{R},k} = \mathbf{cholupdate}\left\{\hat{\boldsymbol{S}}_{\boldsymbol{R},k}, \boldsymbol{y}_k - \boldsymbol{\mathcal{Y}}_{k|k}^{0}, w_0^{(\mathrm{c})}\right\}.$$

IV. Results

The performance of the proposed observer is shown by a validated high fidelity GT-Power model, runtime results, as well as test bench measurement data of the off-road diesel engine. The SS-SR-UKF is implemented as plain C code with a sampling time of $\Delta t = 10\,\mathrm{ms}$.

A. Simulation results

As most quantities to be observed are not measured on the test bench, simulation runs are used to validate the observer performance under high measurement noise. Especially due to the relevance relating to air path control or aftertreatment systems, the observed mass flow rates are of particular importance. According to Sec. II, the mass flow rates directly depend on the states $\boldsymbol{x}$. Consequently, a very good state tracking performance is essential.

Fig. 2 shows the relative tracking error

$$e_i = \frac{\sqrt{\sum_{k=0}^{\tilde{N}} \left(x_i(k) - \hat{x}_i(k)\right)^2}}{\sqrt{\sum_{k=0}^{\tilde{N}} x_i^2(k)}}, \quad i = 1, \ldots, 5, \tag{17}$$

of the states for different Kalman filter configurations, where $\hat{x}_i$ denotes the corresponding estimation. Employing the measurement noise covariance adaptation reduces the relative tracking error by 47 % on average. The resulting relative tracking error for the SS-SR-UKF with adaptation is below 6 %. In addition, the tracking performance of the SS-SR-UKF and SR-UKF is similar.

The trajectories for another (brief) simulation scenario with ramp-shaped changes of the engine speed n_{eng} and torque T_{eng} are shown in Fig. 3. Note that the states are normalized to the maximum boost pressure $\bar{x}_2$ for confidentiality reasons. In order to supply the correct amount of air and exhaust gas for the combustion, the engine controller varies the valve

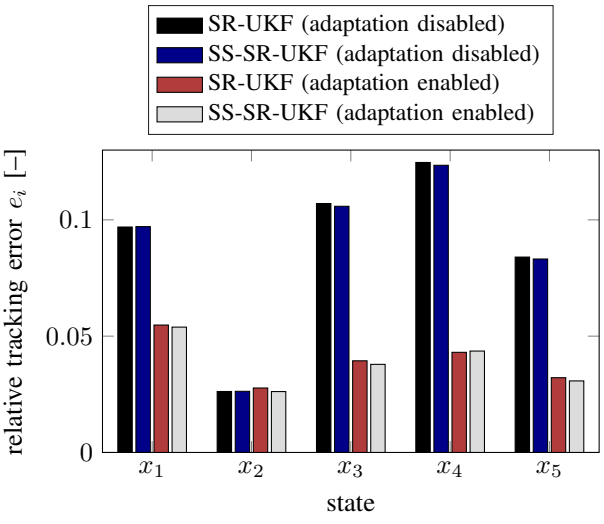

Fig. 2: State tracking errors e_i for different Kalman filter configurations as defined in (17).

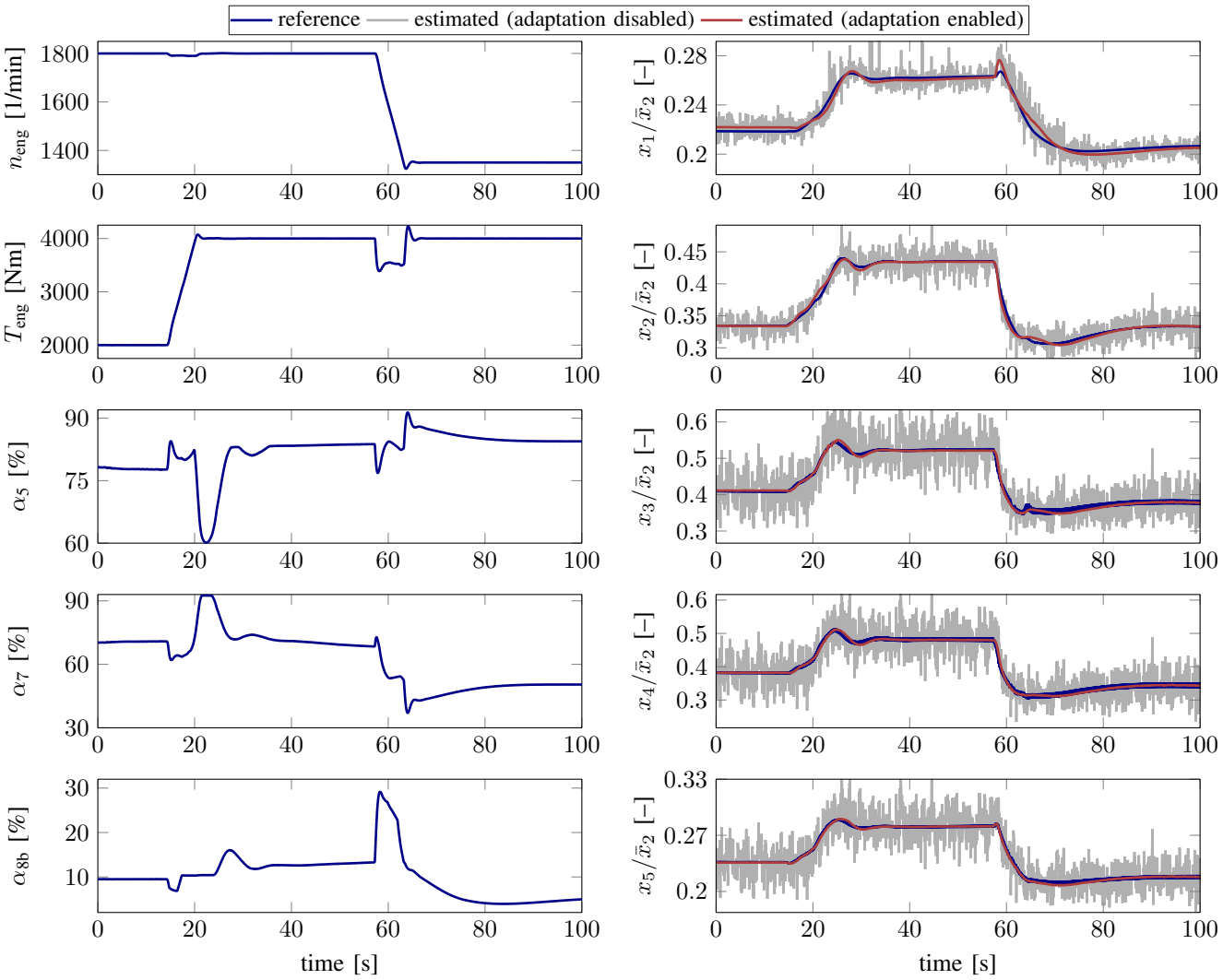

Fig. 3: Pressure tracking performance of the SS-SR-UKF for different engine operating points.

positions $\alpha_j, j \in \{5, 7, 8b\}$. The state tracking performance of the SS-SR-UKF with noise covariance adaptation is very good. Compared to the case without adaptation, the influence of measurement noise is significantly reduced. The simulation starts from a steady-state operation point at an engine speed and torque of 1800 1/min and 2000 Nm. During the first torque change to 4000 Nm at 15 s, all states increase as the higher torque generates a higher exhaust pressure that drives the turbochargers. Similarly, the engine speed change to 1350 1/min at 57 s results in a reduction of all states. Furthermore, the pressure pulsations due to the combustion increase. Note that the reconstructed states (x_3, x_4) are pulsation-free in the noise adaptation case.

B. Computational efficiency

The computation times of the SS-SR-UKF and the SR-UKF (adaptation enabled) were evaluated for a standard laptop and an automotive rapid protoypting system ETAS ES910. The runtime on a typical ECU (MTU ECU 9) is approximately factor three higher. The computation times of both approaches are summarized in Table I. Compared to the SR-UKF, the SS-SR-UKF, is computationally more efficient and renders an equivalent tracking performance. Albeit, the estimated ECU computation time of 9.9 ms for the SR-UKF almost hits the assumed sampling time of 10 ms. As a result, the SS-SR-UKF is to be preferred for an actual ECU realization. Note, however, that the runtime results are primarily in the sense that no hardware-specific optimization steps were applied.

TABLE I: Kalman filter computation times.

hardware	computation time	
	SS-SR-UKF	SR-UKF
Intel Core i7, 2.4 GHz, Win. 8.1	22.9 µs	32.3 µs
ETAS ES910, 800 MHz	2.3 ms	3.3 ms
MTU ADEC (ECU 9)	6.9 ms (est.)	9.9 ms (est.)

C. Measurement results

Testbench measurement data of the off-road diesel engine is used to validate the observer scheme based on the parameters

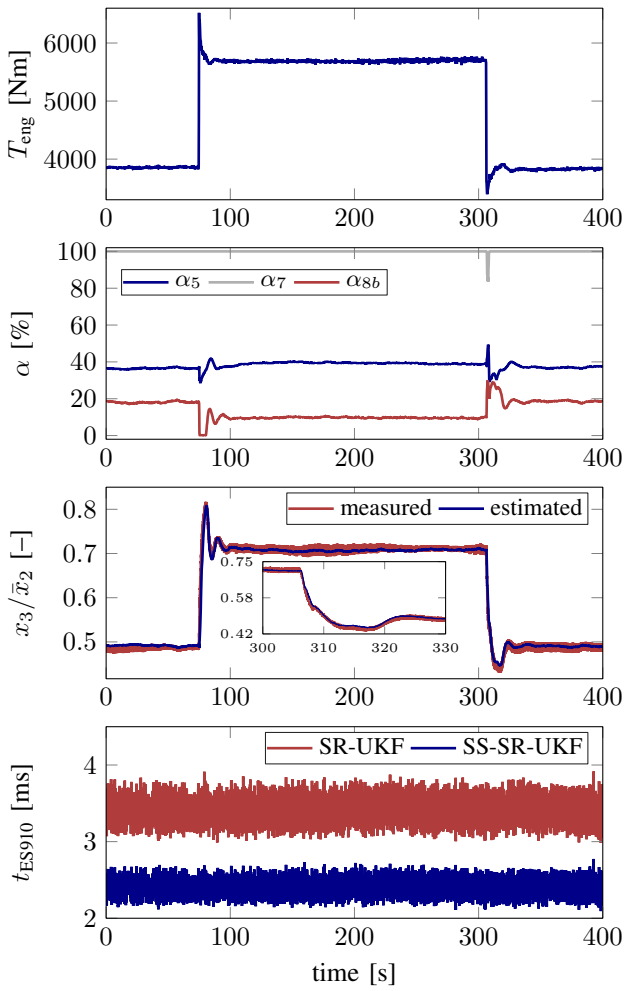

Fig. 4: Exhaust manifold pressure tracking performance for different engine torques at 1800 1/min.

obtained from simulation, e.g. the (fixed) process noise covariance $\boldsymbol{Q}_k$. Unlike a series-produced engine, the testbench engine is equipped with a sensor for the exhaust manifold pressure x_3 that is used for validation.

Fig. 4 shows the corresponding results for a stepwise engine torque changes at a constant speed of 1800 1/min. The first torque change from 4000 Nm to 6000 Nm at 75 s affects the exhaust manifold pressure as well as the flap positions to adjust the new setpoint. The observer perfectly tracks the exhaust pressure trajectory. Equally, the exhaust pressure is tracked for the second torque step back to 4000 Nm at 300 s. Moreover, the estimated trajectory does not contain the typically undesired pressure pulsation noise. Fig. 4 also shows that the corresponding computation times on the rapid prototyping system are almost constant for both approaches.

V. CONCLUSIONS

This paper proposed a tracking approach for the air path pressure states of an off-highway diesel engine. The method is based on a control-oriented nonlinear model for the air path and an experimental model for the nitrous oxides. Based on the computationally efficient engine model, a spherical simplex transform is applied to reduce the numerical effort of the square-root unscented Kalman filter. An nonlinear residual-based noise covariance adaptation scheme is used to increase the robustness concerning modeling errors. Simulation results demonstrate a very low observation error for each state. Subsequently, the verification using testbench measurement data reveals a very good tracking performance for the exhaust manifold pressure. Runtime results additionally indicate the real-time feasibility of the observer on ECU level.

Future work concerns the closed-loop control of the air path based on the observed states and its coupling with a supervised model predictive control for holistic engine operation.

REFERENCES

[1] R. Isermann, *Engine Modeling and Control: Modeling and Electronic Management of Internal Combustion Engines*. Berlin: Springer, 2014.

[2] L. Eriksson and L. Nielsen, *Modeling and Control of Engines and Drivelines*. Hoboken: Wiley, 2014.

[3] L. Guzzella and C. H. Onder, *Introduction to Modeling and Control of Internal Combustion Engine Systems*. Berlin: Springer, 2010.

[4] H. Lee, Y. Park, and M. Sunwoo, "Observer design for exhaust gas recirculation rate estimation in a variable-geometry turbocharger diesel engine using a model reference identification scheme," *Journal of Automobile Engineering*, vol. 228, no. 14, pp. 1688–1699, 2014.

[5] L. E. Kocher, K. Stricker, D. G. V. Alstine, E. Koeberlein, and G. M. Shaver, "Oxygen fraction estimation for diesel engines utilizing variable intake valve actuation," in *Proceedings of the 2012 American Control Conference (ACC)*, Montréal (Canada), 2012, pp. 4963–4968.

[6] F. Castillo, E. Witrant, V. Talon, and L. Dugard, "Simultaneous air fraction and low-pressure EGR mass flow rate estimation for diesel engines," in *Proceedings of the 5th IFAC Symposium on System Structure and Control (SSSC)*, Grenoble (France), 2013, pp. 731–736.

[7] J. Aßfalg, F. Allgöwer, and M. Fritz, "Constrained derivative-free augmented state estimation for a diesel engine air path," in *Proceedings of the 14th IFAC Symposium on System Identification (SYSID)*, Newcastle (Australia), 2006, pp. 1382–1387.

[8] S. Samokhin and K. Zenger, "High-pressure recirculated exhaust gas fraction estimation and control in marine diesel engines," in *Proceedings of the 54th IEEE Conference on Decision and Control (CDC)*, Osaka (Japan), 2015, pp. 1787–1792.

[9] K. Harder, M. Buchholz, J. Niemeyer, J. Remele, and K. Graichen, "A real-time nonlinear MPC scheme with emission constraints for heavy-duty diesel engines," in *Proceedings of the 2017 American Control Conference (ACC)*, Seattle (USA), 2017, pp. 240–245.

[10] R. van der Merwe, "Sigma-point kalman filters for probabilistic inference in dynamic state-space models," Ph.D. dissertation, OGI School of Science & Engineering at Oregon Health & Science University, 4 2004.

[11] S. J. Julier, J. K. Uhlmann, and H. F. Durrant-Whyte, "A new approach for filtering nonlinear systems," in *Proceedings of the 1995 American Control Conference (ACC)*, Seattle (USA), 1995, pp. 1628–1632.

[12] R. V. der Merwe and E. A. Wan, "The square-root unscented kalman filter for state and parameter-estimation," in *Proceedings of the 2001 IEEE International Conference on Acoustics, Speech, and Signal Processing (ICASSP)*, Salt Lake City (USA), 2001, pp. 3461–3464.

[13] S. J. Julier, "The spherical simplex unscented transformation," in *Proceedings of the 2003 American Control Conference (ACC)*, Denver (USA), 2003, pp. 2430–2434.

[14] J. Wang, "Stochastic modeling for real-time kinematic GPS/GLONASS positioning," *NAVIGATION: Journal of the Institute of Navigation*, vol. 46, no. 4, pp. 297–305, 1999.

[15] A. Almagbile, J. Wang, and W. Ding, "Evaluating the performances of adaptive kalman filter methods in GPS/INS integration," *Journal of Global Positioning Systems*, vol. 9, no. 1, pp. 33–40, 2010.

[16] R. Mehra, "On the identification of variances and adaptive kalman filtering," *IEEE Transactions on Automatic Control*, vol. 15, no. 2, pp. 175–184, 1970.

[17] S. J. Julier, "The scaled unscented transformation," in *Proceedings of the 2002 American Control Conference (ACC)*, Anchorage (USA), 2002, pp. 4555–4559.